Constraints of Relic Gravitational Waves by Pulsar Timing Array: Forecasts for the FAST and SKA Projects

Wen Zhao[1,2], Yang Zhang[1,2], Xiao-Peng You[3] and Zong-Hong Zhu[4]

[1]*Department of Astronomy, University of Science and Technology of China, Hefei, 230026, China*
[2]*Key Laboratory for Researches in Galaxies and Cosmology,*
University of Science and Technology of China, Hefei, 230026, China
[3]*School of Physical Science and Techology, Southwest University, Chongqing, 400715, China*
[4]*Department of Astronomy, Beijing Normal University, Beijing 100875, China*

Measurement of the pulsar timing residuals provides a direct way to detect relic gravitational waves at the frequency $f \sim 1/\text{yr}$. In this paper, we investigate the constraints on the inflationary parameters, the tensor-to-scalar ratio r and the tensor spectral index n_t, by the current and future Pulsar Timing Arrays (PTAs). We find that Five-hundred-meter Aperture Spherical radio Telescope (FAST) in China and the planned Square Kilometer Array (SKA) projects have the fairly strong abilities to test the phantom-like inflationary models. If $r = 0.1$, FAST could give the constraint on the spectral index $n_t < 0.56$, and SKA gives $n_t < 0.32$. While an observation with the total time $T = 20$yr, the pulsar noise level $\sigma_w = 30$ns and the monitored pulsar number $n = 200$, could even constrain $n_t < 0.07$. These are much tighter than those inferred from the current results of Parkers Pulsar Timing Array (PPTA), European Pulsar Timing Array (EPTA) and North American Nanohertz Observatory for Gravitational waves (NANOGrav). Especially, by studying the effects of various observational factors on the sensitivies of PTAs, we found that compared with σ_w and n, the total observation time T has the most significant effect.

PACS numbers: 04.30.-w, 04.80.Nn, 98.80.Cq

I. INTRODUCTION

In a whole range of scenarios of the early Universe, including the well-studied inflationary models, a stochastic background of relic (primordial) gravitational waves (RGWs) was produced due to the superadiabatic amplification of zero point quantum fluctuations of the gravitational field [1–3]. Their detection maybe provide the unique way to study the birth of the Universe, the expansion history of Universe before the recombination stage, and test the applicability of general relativity and quantum mechanics in the extremely high-energy scale [4].

Since RGWs have a wide range spreading spectra, from 10^{-18}Hz to 10^{10}Hz, one can detect or constrain them at different frequencies. The temperature and polarization anisotropies of Cosmic Microwave Background (CMB) radiation provide the way to constrain RGWs at very low frequencies, $f < 10^{-15}$Hz. Nowadays, combining with other cosmological observations, the nine-year WMAP data place the constraint on the tensor-to-scalar ratio $r < 0.13$ [5]. While the new Planck data give the the tightest constraint $r < 0.11$ [6], which is equivalent to the constraint of the amplitude of RGWs at lowest frequency $f \sim 10^{-17}$Hz. In the near future, this bound will be greatly improved by the forthcoming polarization observations of Planck satellite, several ground-based and balloon-borne experiments (BICEP, QUIET, POLARBEAR, QUIJOTE, ACTPOL, SPTPOL, QUBIC, EBEX, PIPER, SPIDER et al.), and the planned fourth-generation CMB missions (CMBPol, LiteBird, COrE. et al.).

Among all the direct observations, LIGO S5 has experimentally obtained so far the most stringent bound $\Omega_{\text{gw}} \leq 6.9 \times 10^{-6}$ around $f \sim 100$Hz [7, 8]. It is expected that AdvLIGO, AdvVIRGO, KAGRA, ET and eLISA will also deeply improve it in the near future. In particular, the Planned BBO, DECIGO and ASTROD projects may directly detect the signal of RGWs in the far future. In addition, there are two bounds on the integration $\int \Omega_{\text{gw}}(f)d\ln f \lesssim 1.5 \times 10^{-5}$, obtained by the Big Bang nucleosynthesis (BBN) observation [9] and the CMB observation [10].

By analyzing of pulsar pulse time-of-arrival (TOA) data, people find the millisecond pulsars are very stable clocks. The measurement of their timing residuals provides a direct way to detect GW background in the frequency range $f \in (10^{-9}, 10^{-7})$Hz [11–13]. In addition to the GWs generated by the coalescence of massive black hole binary systems [14] and cosmic strings [15], RGWs are another kind of most important GW sources in this frequency range. Recently, PPTA, EPTA and NANOGrav teams have reported their observational results on the stochastic background of GWs. In [16], by considering these results, we have detailedly investigated the constraints on the Hubble parameter during inflation in the most general scenario for the early Universe. In this paper, we shall extend them to constrain the tensor-to-scalar ratio r and the tensor spectral index n_t.

In addition, as the main goal of this paper, we will discuss the potential constraint (or detection) of RGWs by the future PTA observations. In our discussion, FAST and SKA will be treated as two typical projects, and mainly focused on in the studies. The dependence of the RGWs constraints on the total observation time T, the number of monitored pulsars n and the magnitude of the pulsar timing noise σ_w will be discussed.

This paper is constructed as follows, In Sec. 2, we briefly review the model to describe the RGWs, and relate the energy density of GWs Ω_{gw}, the tensor-to-scalar ratio r and the tensor spectral index n_t to the characteristic strain spectrum $h_c(f)$, which is widely used in the PTA analysis. In Sec. 3, we describe the sensitivities of the current and future experiments, and discuss the dependence on various observational parameters. Sec. 4 summaries the main results of this paper.

II. RELIC GRAVITATIONAL WAVES

Incorporating the perturbation to the spatially flat Friedmann-Robertson-Walker spacetime, the metric is

$$ds^2 = a^2(\eta) \left[d\eta^2 - (\delta_{ij} + h_{ij} dx^i dx^j) \right], \qquad (1)$$

where a is the scale factor of the universe, and η is the conformal time, which relates to the cosmic time by $a d\eta = dt$. The perturbation of spacetime h_{ij} is a 3×3 symmetric matrix. The gravitational-wave field is the tensorial portion of h_{ij}, which is transverse-traceless $\partial_i h^{ij} = 0$, $\delta^{ij} h_{ij} = 0$.

RGWs satisfy the linearized evolution equation [1]:

$$\partial_\mu(\sqrt{-g} \partial^\mu h_{ij}) = -16\pi G \pi_{ij}. \qquad (2)$$

The anisotropic portion π_{ij} is the source term, which can be given by the relativistic free-streaming gas [17]. However, it has been deeply discussed that the relativistic free-streaming gas, such as the decoupled neutrino, can only affect the RGWs at the frequency range $f \in (10^{-16},\ 10^{-10})$Hz, which could be detected by the future CMB observations [18]. So, it cannot obviously influence the RGWs at the frequency $f \in (10^{-9},\ 10^{-7})$Hz. For this reason, in this paper we shall ignore the contribution of the external sources. So the evolution of RGWs only depends on the scale factor and its time derivative.

It is convenient to Fourier transform the equation as follows:

$$h_{ij}(\eta, \vec{x}) = \int \frac{d^3\vec{k}}{(2\pi)^{3/2}} \sum_{s=+,\times} \left[h_k(\eta) \epsilon_{ij}^{(s)} c_{\vec{k}}^{(s)} e^{i\vec{k}\cdot\vec{x}} + c.c. \right], \qquad (3)$$

where $c.c.$ stands for the complex conjugate term. The polarization tensors are symmetry, transverse-traceless $k^i \epsilon_{ij}^{(s)}(\vec{k}) = 0$, $\delta^{ij} \epsilon_{ij}^{(s)}(\vec{k}) = 0$, and satisfy the conditions $\epsilon^{(s)ij}(\vec{k})\epsilon_{ij}^{(s')}(\vec{k}) = 2\delta_{ss'}$ and $\epsilon_{ij}^{(s)}(-\vec{k}) = \epsilon_{ij}^{(s)}(\vec{k})$. Since the RGWs we will consider are isotropy, and each polarization state is the same, we have denoted $h_{\vec{k}}^{(s)}(\eta)$ by $h_k(\eta)$, where $k = |\vec{k}|$ is the wavenumber of the GWs, which relates to the frequency by $k \equiv 2\pi f$. (The present scale factor is set $a_0 = 1$). So Eq.(2) can be rewritten as

$$h_k'' + 2\frac{a'}{a} h_k' + k^2 h_k = 0, \qquad (4)$$

where the *prime* indicates a conformal time derivative $d/d\eta$. For a given wavenumber k and a given time η, we can define the transfer function t_f as

$$t_f(\eta, k) \equiv h_k(\eta)/h_k(\eta_i), \qquad (5)$$

where η_i is the initial time. This transfer function can be obtained by solving the evolution equation (4).

The strength of the GWs is characterized by the GW energy spectrum, $\Omega_{\mathrm{gw}} \equiv \rho_{\mathrm{gw}}/\rho_0$, where $\rho_{\mathrm{gw}} = \frac{1}{32\pi G} \langle \dot{h}_{ij} \dot{h}^{ij} \rangle$, the critical density is $\rho_0 = \frac{3H_0^2}{8\pi G}$, and H_0 is the current Hubble constant. Using Equations in (3) and (5), the energy density of GWs can be written as [19]

$$\rho_{\mathrm{gw}} = \int \frac{dk}{k} \frac{P_t(k) \dot{t}_f^2(\eta_0, k)}{32\pi G}, \qquad (6)$$

where $P_t(k) \equiv \frac{2k^3}{\pi^2}|h_k(\eta_i)|^2$ is the so-called primordial power spectrum of RGWs. Thus, we derive that the current energy density of RGWs,

$$\Omega_{\mathrm{gw}} \equiv \int \Omega_{\mathrm{gw}}(k) d\ln k,\ \text{and}\ \Omega_{\mathrm{gw}}(k) = \frac{P_t(k)}{12H_0^2} \dot{t}_f^2(\eta_0, k), \qquad (7)$$

where the *dot* indicates a cosmic time derivative d/dt.

Now, let us discuss the terms $P_t(k)$ and $t_f(\eta_0, k)$ separately. The primordial power spectrum of RGWs is usually assumed to be power-law as follows:

$$P_t(k) = A_t(k_*) \left(\frac{k}{k_*} \right)^{n_t}. \qquad (8)$$

This is a generic prediction of a wide range of scenarios of the early Universe, including the inflation models. $A_t(k_*) = \frac{16H_*^2}{\pi m_{\mathrm{Pl}}^2}$ directly relates to the value of Hubble parameter H at time when wavelengths corresponding to the wavenumber k_* crossed the horizon [1, 3, 16, 20]. In observations, we always define the tensor-to-scalar ratio r, and write the amplitude of RGWs as $A_t(k_*) = A_s r$, where A_s is the amplitude of primordial density perturbation at $k = k_*$. n_t is the spectral index of RGWs, which relates to the effective equation-of-state w of the cosmic "matter" in the inflationary stage by the relation,

$$n_t = \frac{4}{1+3w} + 2. \qquad (9)$$

If the inflation is an exact de Sitter expansion stage with $w = -1$, we have the scale-invariant spectrum with $n_t = 0$. For the canonical scalar-field inflationary models, we have $w > -1$, which predicts the red spectrum of RGWs with $n_t < 0$ [3]. However, for the phantom inflationary models [21], one has $w < -1$ and $n_t > 0$. So the determination of n_t can distinguish different kinds of inflationary scenarios.

Now, let us turn to the transfer function t_f, defined in (5), which describes the evolution of GWs in the expanding Universe. From Eq.(4), we find that this transfer

function can be directly derived, so long as the scale factor as a function of time is given [22–26]. In this paper, we shall use the following analytical approximation for this transfer function. It has been known that, during the expansion of the Universe, the mode function $h_k(\eta)$ of the GWs behaves differently in two regions [22]. When waves are far outside the horizon, i.e. $k \ll aH$, the amplitude of h_k keeps constant, and when inside the horizon, i.e. $k \gg aH$, the amplitude is damping with the expansion of Universe, i.e., $h_k \propto 1/a(\eta)$. In the standard hot big-bang cosmological model, we assume that the inflationary stage is followed by a radiation dominant stage, and then the matter dominant stage and the Λ dominant stage. In this scenario, by numerically integrating Eq.(4), one finds that the damping function $\dot{t}_f$ can be approximately described by the following form [27–30]

$$\dot{t}_f(\eta_0, k) = \frac{-3j_2(k\eta_0)\Omega_m}{k\eta_0}\sqrt{1 + 1.36(\frac{k}{k_{eq}}) + 2.50(\frac{k}{k_{eq}})^2},$$ (10)

where $k_{eq} = 0.073\Omega_m h^2 \text{Mpc}^{-1}$ is the wavenumber corresponding the Hubble radius at the time that matter and radiation have equal energy density, and $\eta_0 = 1.41 \times 10^4 \text{Mpc}$ is the present conformal time. The factor Ω_m encodes the damping effect due to the recent accelerating expansion of the Universe [23, 24, 27]. In this damping factor, we have ignored the small effects of neutrino free-streaming [17] and various phase transitions in the early Universe [26]. In this paper, we shall focus on the wavenumber $k \gg k_{eq}$. In this range, we have the current density of RGWs as follows,

$$\Omega_{\text{gw}}(k) = \frac{15}{16}\frac{\Omega_m^2 A_s r}{H_0^2 \eta_0^4 k_{eq}^2}\left(\frac{k}{k_*}\right)^{n_t},$$ (11)

which clearly presents the dependence of the RGWs on various cosmological parameters.

In the PTA analysis, people always describe the GW background by the characteristic strain spectrum $h_c(f)$ [31]. For most models of interest, it can be written as a power-law dependence on frequency f:

$$h_c(f) = A\left(\frac{f}{\text{yr}^{-1}}\right)^{\alpha}.$$ (12)

The characteristic strains relate to one-side power spectrum $P(f)$ and the energy density of GWs $\Omega_{\text{gw}}(f)$ as

$$P(f) = \frac{h_c^2(f)}{12\pi^2 f^3}, \quad \Omega_{\text{gw}}(f) = \frac{2\pi^2}{3H_0^2}f^2 h_c^2(f).$$ (13)

Comparing the Equations in (11) and (13), we find that

$$\alpha = \frac{n_t}{2} - 1,$$ (14)

and

$$\frac{A}{\text{yr}} = \sqrt{\frac{45}{32\pi^2}\frac{\Omega_m^2 A_s r}{\eta_0^4 k_{eq}^2}}\left(\frac{\text{yr}^{-1}}{f_*}\right)^{n_t}.$$ (15)

Considering the cosmological parameters based on the current Planck observations [6] $h = 0.6711$, $\Omega_m = 0.3175$, $\Omega_\Lambda = 0.6825$, $z_{eq} = 3402$, $A_s = 2.495 \times 10^{-9}$ at $k_* = 0.002\text{Mpc}^{-1}$ [32], we obtain that

$$A = 0.88\sqrt{r} \times 10^{5n_t - 18},$$ (16)

and

$$\Omega_{\text{gw}}(f) = 1.09r \times 10^{10n_t - 15}\left(f/\text{yr}^{-1}\right)^{n_t}.$$ (17)

These relations will be used for the following discussion. Both Equations in (16) and (17) show that the amplitude of RGWs at $f \sim 1/\text{yr}$ strongly depends on the spectral index n_t. For the cases with the scale-invariant and red spectrum, one always has $A \lesssim 10^{-18}$ and $\Omega_{\text{gw}} \lesssim 10^{-15}$. However, for the cases with blue spectrum, i.e. $n_t > 0$, the values of A and Ω_{gw} can be dramatically large. For example, in the models suggested by Grishchuk [33], the blue spectrum with $\alpha \in [-0.8, -1]$ was expected, which corresponds to $n_t \in [0, 0.4]$, the amplitude of RGWs could be $A \sim 10^{-17}$ and $\Omega_{\text{gw}} \sim 10^{-14}$.

III. PULSAR TIMING ARRAY AND THE DETECTION OF RELIC GRAVITATIONAL WAVES

A. Current constraints

In 2006, Jenet et al. have analyzed the PPTA data and archival Arecibo data for several millisecond pulsars. By focusing on the GWs at the frequency $f = 1/\text{yr}$, the authors obtained the 2σ upper limit on A as a function of the spectral slope α, which is presented in the left panel of Fig.1 (black solid line) [34]. Recently, this upper limit has been updated by EPTA and NANOGrav teams [35, 36]. It is interesting that in [34], the authors have also investigated the possible upper limit (or a definitive detection) of stochastic background of GWs by using the potential completed PPTA data-sets (20 pulsars with an rms timing residual of 100ns over 5 years, which is also expected the case for future EPTA and NANOGrav projects). We have also plotted the current EPTA upper limit (blue dashed line), current NANOGrav upper limit (green dash-dotted line) and the potential PPTA upper limit of parameter A in the left panel of Fig.1 (red dotted line).

By using the relations in Eqs. (14) and (16), we obtain the constraints on the parameters r and n_t, which are presented in the right panel of Fig.1. Note that the regions above the lines are excluded by the corresponding PTA observations. We notice that the current Planck observations give the tightest constraint $r < 0.11$ [6], which is nearly independent of the spectral index n_t [37, 38]. So, combining with Planck constraint on r, this figure shows the current allowed region in the r-n_t plane. For example, if $r = 0.1$ is determined by the forthcoming CMB observations, current PPTA gives the constraint $n_t < 0.94$,
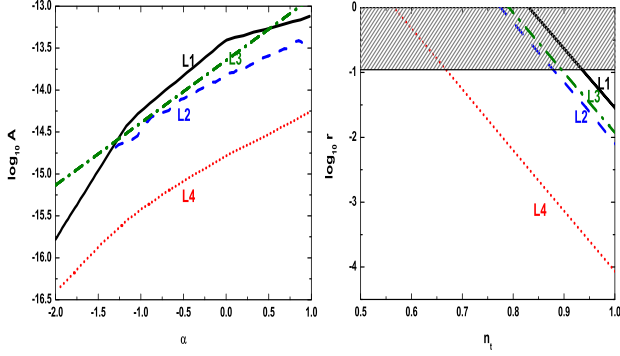
FIG. 1: Left panel: The upper limit of A as a function of the spectral slope α. Right panel: The upper limit of r for any given n_t, where the shaded region is excluded by the current Planck observations. In each panel, the black solid line (i.e. L1) is for current PPTA 2σ result [34], the blue dashed line (i.e. L2) is for current EPTA 2σ result [35], the green dash-dotted line (i.e. L3) is for current NANOGrav 2σ result [36] and the red dotted line (i.e. L4) is for future PPTA 2σ result [34].

NANOGrav gives $n_t < 0.90$ and EPTA gives $n_t < 0.88$ at 2σ confident level. Meanwhile, the future PPTA will follow the constraint of $n_t < 0.67$. These are listed in Table I. Although quite loose, these constraints would be helpful to exclude some inflationary models with very blue GW spectrum.

From Fig.1 and Eq.(17), we can also obtain the constraints on the energy density of RGWs $\Omega_{\mathrm{gw}}(f)$. For instance, if $n_t = 0$ and $f = 1/\mathrm{yr}$ are fixed, the upper limits for $\Omega_{\mathrm{gw}}(f)$ are listed in Table II, which are consistent with the results in [34–36].

B. Detecting GW background by Pulsar Timing Array

In the following discussion, we shall study the potential constraints on the RGWs by the future PTA observations, where we will focus on the Chinese FAST project and the planned SKA project.

The fluctuations of the pulsar TOAs caused by the stochastic GW background are random. However, for different pulsars, these fluctuations have the correlations. Let us assume the observations of $n \gg 1$ pulsars at times t_0, t_1, ..., t_{m-1} with the time interval Δt. The total observation time is $T = m\Delta t$. We denote the timing residual of i-th pulsar at time t_k as R_k^i, which includes the contribution from both GWs s_k^i and the noises n_k^i, i.e. $R_k^i = s_k^i + n_k^i$.

For the isotropic GW background, the correlation between the GW-induced signals are [12, 39, 40]

$$\langle s_k^i s_{k'}^j \rangle = \sigma_g^2 H_{ij} \gamma_{kk'}, \tag{18}$$

where σ_g is the root mean square (RMS) of the timing residuals induced by GW background, which relates to the one-side power spectrum $P(f)$ by $\sigma_g^2 = \int_{f_l}^{f_h} P(f)df$. The highest and lowest frequency of GWs are given by $f_h = \frac{1}{2\Delta t}$ and $f_l = \frac{1}{T}$. H_{ij} is the so-called Hellings-Downs function, which is given by $H_{ij} = \frac{3}{2}x \ln x - \frac{x}{4} + \frac{1}{2}(1+\delta(x))$, where $x = \frac{1-\cos(\theta)}{2}$ and θ is the angle distance between i-th and j-th pulsar. $\gamma_{kk'}$ is the temporal correlation coefficient between the k-th and k'-th sampling.

The noise term n_k^i includes the effects of all non-GW sources for the i-th pulsar. It is assumed that all noise sources have a flat spectrum, which is consistent with most observations [39]. In order to simplify the problem, in this paper, we assume all monitored pulsars have the same noise level, i.e.

$$\langle n_k^i n_{k'}^j \rangle = \sigma_w^2 \delta_{ij} \delta_{kk'}. \tag{19}$$

There are several methods to extract the GW signals from the observable R_k^i [39, 41, 42]. In this paper, we follow the method suggested by Jenet et al. in 2005 [39]. In particular, we shall present the details of the calculation, which are quite helpful to understand the method, but have been neglected in the original paper [39]. In addition, some sub-dominant terms, which were neglected in [39], will also be presented in the finial formulas. We calculate the correlation coefficient between the observed timing residuals of each pair of observed pulsars:

$$c_{ij} = \frac{1}{m} \sum_{k=1}^m R_k^i R_k^j. \tag{20}$$

It is easy to get the expected values of c_{ij} and c_{ij}^2,

$$\langle c_{ij} \rangle = \sigma_g^2 H_{ij}, \tag{21}$$

$$\langle c_{ij}^2 \rangle = \sigma_g^4 \left(H_{ij}^2 + \frac{(1+H_{ij}^2)\chi}{m} + \frac{2\sigma_w^2}{m\sigma_g^2} + \frac{4\sigma_w^4}{m\sigma_g^4} \right), \tag{22}$$

where $\chi = \sum_{kk'} \gamma_{kk'}^2/m$, and $\langle \cdot \rangle$ denotes the ensemble average.

The comparison between c_{ij} and the Hellings-Downs function is carried out by defining the GW detection significance S as follows,

$$S = \frac{\sqrt{N} \sum_{i-j} (c_{ij} - \overline{c})(H_{ij} - \overline{H})}{\sqrt{\sum_{i-j} (c_{ij} - \overline{c})^2 \sum_{i-j} (H_{ij} - \overline{H})^2}}, \tag{23}$$

where $N = n(n-1)/2$ is the number of independent pulsar pairs. The summation $\sum_{i-j}$ sums over all independent pulsar pairs, i.e. $\sum_{i-j} \equiv \sum_{i=1}^n \sum_{j=1}^{i-1}$. The

TABLE I: The 2σ upper limit of the spectral index n_t inferred from various pulsar timing observations.

	Current PPTA	Current EPTA	Current NANOGrav	Future PPTA	FAST	SKA	Optimal Case
$r = 0.1$	0.94	0.88	0.90	0.67	0.56	0.32	0.07
$r = 0.01$	> 1	0.99	> 1	0.78	0.67	0.44	0.18
$r = 0.001$	> 1	> 1	> 1	0.89	0.77	0.55	0.31

TABLE II: The 2σ upper limit of the energy density $\log_{10}\left[\Omega_{\mathrm{gw}}(f = \mathrm{yr}^{-1})\right]$ inferred from various pulsar timing observations, where we have set $n_t = 0$, i.e. $\alpha = -1$.

Current PPTA	Current EPTA	Current NANOGrav	Future PPTA	FAST	SKA	Optimal Case
-7.36	-7.79	-7.63	-9.84	-10.63	-12.99	-15.30

quantities $\overline{c}$ and $\overline{H}$ are defined as

$$\overline{c} = \frac{1}{N}\sum_{i-j} c_{ij}, \quad \overline{H} = \frac{1}{N}\sum_{i-j} H_{ij}. \quad (24)$$

To evaluate the quality of the detector, we need the expected value $\langle S\rangle$, which is $\langle S\rangle \simeq \sqrt{N}\sigma_g^2 \Sigma_H/\Sigma_c$, where

$$\Sigma_H^2 = \frac{1}{N}\sum_{i-j}(H_{ij} - \overline{H})^2, \quad \Sigma_c^2 = \frac{1}{N}\sum_{i-j}(c_{ij} - \overline{\langle c\rangle})^2. \quad (25)$$

By using Eqs. (21) and (22), we get the well-known result,

$$\langle S\rangle \simeq \sqrt{N}\left[1 + \frac{\chi(1 + \overline{H^2}) + \frac{2\sigma_w^2}{\sigma_g^2} + \frac{4\sigma_w^4}{\sigma_g^4}}{m\Sigma_H^2}\right]^{-1/2}. \quad (26)$$

In Jenet et al. (2005), this formula was obtained by another way, which is easier to extend to the results after low-pass filtering and whitening. It is convenient to define the expected discrete power spectrum of R_k^i for the i-th pulsar $P_d(\Delta, i)$, which includes both a GW component and a white noise component, i.e. $P_d(\Delta, i) = P_g(\Delta) + \frac{\sigma_w^2(i)}{m}$. Note that $\Delta > 0$ is the discrete frequency bin number corresponding to frequency Δ/T. Since we have assumed that σ_w has the same value for every pulsar, the spectrum $P_d(\Delta, i)$ becomes independent of i, so we denote it as $P_d(\Delta)$ in the following discussion. For the GW with the characteristic strain spectrum $h_c(f)$ in Eq.(12), one has the discrete GW-induced spectrum as follows,

$$P_g(\Delta) = \frac{(A \cdot \mathrm{yr})^2(T/\mathrm{yr})^{2-2\alpha}}{(2\pi)^2(2 - 2\alpha)}m(\Delta), \quad (27)$$

where $m(\Delta = 1) = \beta^{2\alpha-2} - 1.5^{2\alpha-2}$, and $m(\Delta > 1) = (\Delta - 0.5)^{2\alpha-2} - (\Delta + 0.5)^{2\alpha-2}$. $\beta \simeq 1$ is the lowest frequency used to calculate the correlation function c_{ij}. According to the Wiener-Khinchin theorem and the defini-

tion of Σ_c, we find that

$$\Sigma_c^2 = \sigma_g^4\Sigma_H^2 + \sum_\Delta P_d^2(\Delta) + \overline{H^2}\sum_\Delta P_g^2(\Delta)$$

$$= \sigma_g^4\Sigma_H^2 + (1 + \overline{H^2})\sum_\Delta P_g^2(\Delta) + \sigma_g^4\left(\frac{2\sigma_w^2}{\sigma_g^2} + \frac{\sigma_w^4}{\sigma_g^4}\right),$$

and the quantity χ is calculated by $\frac{\chi}{m} = \frac{1}{\sigma_g^4}\sum_\Delta P_g^2(\Delta)$, which can be gotten for any given GW background. By using the relation $\langle S\rangle \simeq \sqrt{N}\sigma_g^2\Sigma_H/\Sigma_c$, we can naturally obtain the result in Eq. (26).

In order to enhance the detection significance, the low-pass filtering and whitening techniques can be applied [39]. In this way, we can correlate only that part of signal which has a high signal-to-noise ratio and give each time series a flat spectrum to optimize the measurement of the correlation function. In practice, we define the new discrete power spectrum $\hat{P}_d(\Delta)$ and $\hat{P}_g(\Delta)$ as follows,

$$\hat{P}_d(\Delta) = \frac{P_d(\Delta)}{P_d(\Delta)}\frac{\sigma_d^2}{m}, \quad \hat{P}_g(\Delta) = \frac{P_g(\Delta)}{P_d(\Delta)}\frac{\sigma_d^2}{m}, \quad (28)$$

where $\sigma_d^2 = \sum_\Delta P_d(\Delta)$. In this definition, the total RMS fluctuation induced by GW becomes $\hat{\sigma}_g^2 = \sum_{\Delta=1}^{\Delta_{\max}}\hat{P}_g(\Delta)$, where the summation is carried out only over the frequency bins in which the GW signal dominates the noise, and $\Delta_{\max}$ is the number of the highest frequency bin. So the variance Σ_c becomes

$$\Sigma_c^2 = \hat{\sigma}_g^4\Sigma_H^2 + \sum_\Delta \hat{P}_d^2(\Delta) + \overline{H^2}\sum_\Delta \hat{P}_g^2(\Delta) \quad (29)$$

$$= \hat{\sigma}_g^4\Sigma_H^2 + \frac{\sigma_d^4}{m^2}\left[\sum_{\Delta=1}^{\Delta_{\max}}\left(1 + \left(\frac{P_g(\Delta)}{P_d(\Delta)}\right)^2\overline{H^2}\right)\right], \quad (30)$$

and the expected value of S becomes

$$\langle S\rangle \simeq \sqrt{N}\left[1 + \frac{\sum_{\Delta=1}^{\Delta_{\max}}\left(1 + \left(\frac{P_g(\Delta)}{P_d(\Delta)}\right)^2\overline{H^2}\right)}{\left(\sum_{\Delta=1}^{\Delta_{\max}}\frac{P_g(\Delta)}{P_d(\Delta)}\right)^2\Sigma_H^2}\right]^{-1/2}. \quad (31)$$

This formula will be used in the following subsection.

C.   Forecasts for FAST and SKA projects

FAST is a Chinese megascience project to build the largest single dish radio telescope in the world. Funding for FAST has been approved in 2007, and its first light is expected to be in 2016 [43]. It includes multibeam and multiband, covering a frequency range of 70MHz−3GHz. The relatively low latitude ($\sim 26°$N) of the site enables the observation of more southern galactic pulsars. The zenith angle of FAST is about $40°$, which corresponds to $\overline{H^2} = 0.024$ and $\Sigma_H = 0.155$, if assuming the monitored millisecond pulsars evenly distribute in the observed region. One of the scientific goals of FAST is to discover ~ 400 new millisecond pulsars. FAST is capable of providing the most precise observations of pulsar timing signals, therefore, may largely increase the sensitivity of the spectrum window for detection of GWs.

The noise level of the millisecond pulsars are expected to be $\sigma_w = 30$ns, after collecting the timing data for the total time $T = 5$yr [43]. As a conservative evaluate, similar to PPTA, we assume FAST will monitor 20 pulsars for the detection of GWs. Thus, by using Eq.(31), we can calculate the detection significance S for any given RGW models, which are illustrated in Fig.2. In this figure, we have considered three typical models with $r = 0.1$, 0.01 and 0.001. These models are predicted by the general inflationary models, and could be well detected by the future CMB observations [44]. As anticipated, if $n_t < 0$, we always have $S \ll 1$, i.e. the detection is impossible for the red spectrum of RGWs. However, if the RGWs have the blue spectrum, the detection is possible. For instance, for the model with $r = 0.1$ and $n_t = 0.56$ or for that with $r = 0.01$ and $n_t = 0.67$, FAST can detect the signal of RGWs at 2σ level. In Fig.3, we set $\langle S \rangle = 2$, and plot the value of r for any spectral index n_t. Comparing those in the right panel of Fig.1, we find that FAST is much more sensitive than current and future PPTA and/or EPTA.

As another potential observation, we consider SKA project, which is a proposed major internationally-funded radio telescope, and is expected to be completed in the next decade [45]. SKA will consist of many antennas, constituting an effective collecting area of about one square kilometer. We expect that SKA will survey the full sky. If assuming the monitored millisecond pulsars are evenly distributed, we have $\overline{H^2} = \Sigma_H^2 = 1/48$, which are slightly different from those of FAST. Following [46], we assume SKA will select 100 pulsars and spend the total time $T = 10$yr for the GW detection, and the average noise level of these pulsars are about $\sigma_w = 50$ns, which is 2 times lower than those the finial PPTA, EPTA or NANOGrav. In Fig.2, we consider the typical inflationary models with $r = 0.1$, 0.01 and 0.001, and plot the values of S for any n_t. Again, we find the detection is possible, only if $n_t > 0$, i.e. the blue GW spectrum. Compared with the results of FAST, the detection significance are much higher, due to the longer observation time T and the larger pulsar number n. These are also
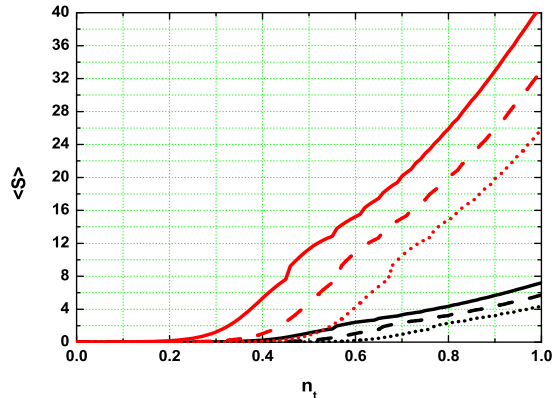

FIG. 2: The detection significance of RGWs for FAST (dark lines, black online) and SKA (gery lines, red online) projects. For FAST, we have assumed $T = 5$yr, $\sigma_w = 30$ns, and $n = 20$, and for SKA we have assumed $T = 10$yr, $\sigma_w = 50$ns, and $n = 100$. For both cases, solid lines are for the models with $r = 0.1$, dashed lines are for $r = 0.01$, and dotted lines are for $r = 0.001$.

clearly shown in Fig.3 and Table I. In Table II, we have listed the detection limits of the energy density $\Omega_{\rm gw}$ for the FAST and SKA projects, where we also find that SKA is more sensitive than FAST.

From the formula in Eq.(31), we know that the detection significance of PTA projects mainly depends on three factors: the total observation time T, the number of the monitored millisecond pulsars n and the noise level of the pulsar σ_w [47]. Now, let us discuss the dependence of sensitivity on these factors separately. First, we fix $\sigma_w = 50$ns and $n = 100$, and investigate the effect of observation time T. To do it, we consider three cases with $T = 5$yr, 10yr and 20yr. Setting the detection significance $\langle S \rangle = 2$, we plot the constraints of the inflationary models in the r-n_t plane in Fig.4, where we find the effect of total time T is very significant. For example, for the model with $r = 0.1$, the 5yr observations give the constraint $n_t < 0.48$, which can be improved to $n_t < 0.17$ for the 20yr observations. For comparison, in this figure, we have also consider the optimal case, where $\sigma_w = 30$ns, $n = 200$ and $T = 20$yr are assumed. We find that, in this optimal case, the constraint of spectral index is only slightly improved to $n_t < 0.07$, although the noise level and pulsar numbers are greatly improved.

This effect can be understood by the following analysis. As well known, the contributions of GWs on the pulsar timing residuals mainly come from those at the lowest frequency range, i.e. $f \sim f_l$. So the detection significance S sensitively depends on the f_l value. At the same time, we know that $f_l = 1/T$. So the larger total observation time T corresponds to the smaller f_l value, which means that more low-frequency GWs can contribute the timing
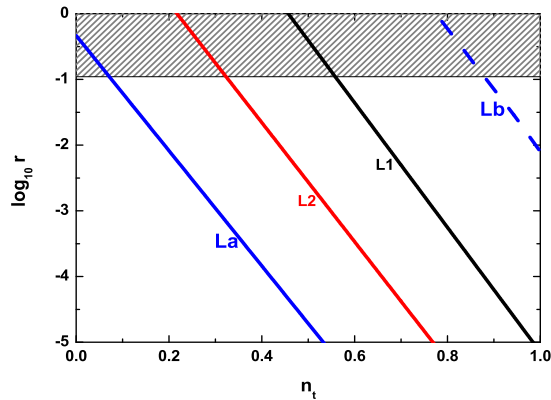
FIG. 3: The upper limits of r and n_t based on the potential FAST observations (black line, i.e. L1) and SKA observations (red line, i.e. L2). Note that the shaded region is excluded by current Planck observations. The dashed blue line (i.e. Lb) is the current tightest constraint coming from the EPTA observations, which is identical to that in the right panel of Fig. 1. The solid blue line (i.e. La) indicates the result in the optimal case considered in this paper, where $T = 20$yr, $\sigma_w = 30$ns, and $n = 200$ are assumed.

FIG. 4: The upper limits of r and n_t depend on the total observation time T. The solid black line (i.e. L2) is for the case with $T = 5$yr, dashed black line (i.e. L1) is for $T = 10$yr, and dotted black line (i.e. L3) is for $T = 20$yr. In all cases, $\sigma_w = 50$ns and $n = 100$ are assumed. The solid blue line (i.e. La) and dashed blue line (i.e. Lb) are identical to those in Fig.3. The dashed black line (i.e. L1) is identical to that for SKA.

residuals of pulsars. This explains why the observation time T is the most important factor for the sensitivity of PTA.

Second, we study the effect of noise level of pulsars σ_w. Decreasing σ_w is equivalent to increasing the $\Delta_{\max}$ value. So a smaller σ_w corresponds to the case where more high-frequency GWs have the contributions to the pulsar timing residuals. However, we know that, compared with the low-frequency GWs, the high-frequency ones are much less important for the timing residuals. The results are shown in Fig.5, where three cases with $\sigma_w = 100$ns, 50ns and 30ns are considered. Although as anticipated, lower σ_w corresponds to the higher sensitivity of PTA, the effect of σ_w is less significant than that of observation time T.

Third, the pulsar number n affects the value of S only by the factor $\sqrt{N}$ in Eq.(31), which follows that $\langle S \rangle \propto n$ for $n \gg 1$. This effect is illustrated in Fig.6, where three cases with $n = 50$, 100 and 200 are considered. We find that, compared with the total observation time T and the pulsar noise level σ_w, the pulsar number n has the relatively smaller influence on the detection significance S.

IV. CONCLUSIONS

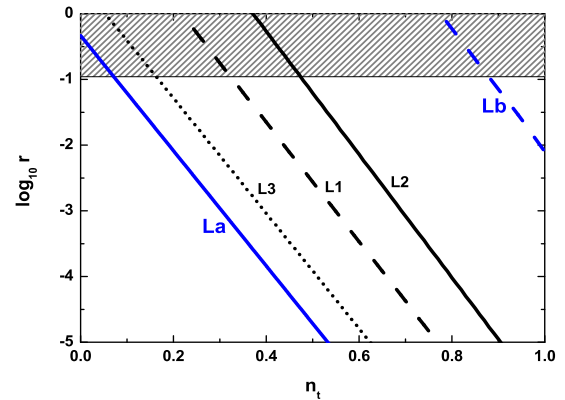Generation of GW background in the early inflationary stage is a necessity dictated by general relativity and quantum mechanics. The wide range spreading spectra of RGWs make the possible detection at different frequency ranges by various methods. The timing studies of the millisecond pulsars provide a unique way to constrain it in the middle frequency range $f \in (10^{-9}, 10^{-7})$Hz.

Recently, PPTA, EPTA and NANOGrav teams have reported their observational results on GW background at $f \sim 1/$yr. In this paper, we infer from these bounds the constraint of inflation in r-n_t plane. Although quite loose, these constraints are helpful to exclude some phantom-like inflationary models.

As the main goal of this paper, we have forecasted the future pulsar timing observations and the potential constraints on inflationary parameters r and n_t, by focusing on the FAST and SKA projects. We found that, if $r = 0.1$, FAST could give the constraint on the spectral index $n_t < 0.56$, and SKA gives $n_t < 0.32$. While an observation with the total time $T = 20$yr, the pulsar noise level $\sigma_w = 30$ns and the monitored pulsar number $n = 200$, could even constrain $n_t < 0.07$, which can exclude or test most phantom-like inflationary models with this tensor-to-scalar ratio. In this paper, we have also studied the effects of T, σ_w and n on the sensitivity of PTA, and found that the total observation time T has the most important influence. So increasing the observation time can significantly improve the sensitivities of the future PTAs.
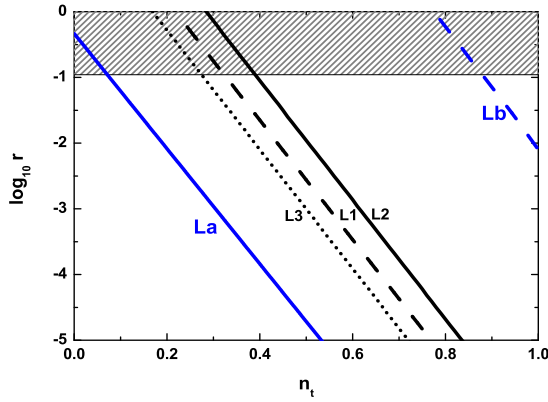
FIG. 5: The upper limits of r and n_t depend on the noise level σ_w. The solid black line (i.e. L2) is for the case with $\sigma_w = 100$ns, dashed black line (i.e. L1) is for $\sigma_w = 50$ns, and dotted black line (i.e. L3) is for $\sigma_w = 30$ns. In all cases, $T = 10$yr and $n = 100$ are assumed. The solid blue line (i.e. La) and dashed blue line (i.e. Lb) are identical to those in Fig.3. The dashed black line (i.e. L1) is identical to that for SKA.

[1] L.P. Grishchuk, Sov. Phys. JETP **40**, 409 (1975); Ann. N. Y. Acad. Sci. **302**, 439 (1977); JETP Lett. **23**, 293 (1976);
[2] A.A. Starobinsky, JETP Lett. **30**, 682 (1979); Phys. Lett. B**91**, 99 (1980).
[3] A.D. Linde, Phys. Lett. B**108**, 389 (1982); A. Albrecht and P.J. Steinhardt, Phys. Rev. Lett. **48**, 1220 (1982); V.F. Mukhanov, H.A. Feldman, and R.H. Brandenberger, Phys. Rep. **215**, 203 (1992); D.H. Lyth and A. Riotto, Phys. Rep. **314**, 1 (1999).
[4] L.P. Grishchuk, arXiv:0707.3319.
[5] G. Hinshaw et al., arXiv:1212.5226.
[6] Planck Collaboration, arXiv:1303.5076.
[7] B.P. Abbott et al., [LIGO Scientific Collaboration and Virgo Collaboration], Nature, **460**, 990 (2009).
[8] Y. Zhang, M.L. Tong and Z.W. Fu, Phys. Rev. D**81**, 101501(R) (2010).
[9] B. Allen and J.D. Romano, Phys. Rev. D**59**, 102001 (1999).
[10] T.L. Smith, E. Pierpaoli, and M. Kamionkowski, Phys. Rev. Lett. 97, 021301 (2006).
[11] S. Detweiler, Astrophys. J. **234**, 1100 (1979).
[12] R.W. Hellings and G.S. Downs, Astrophys. J. **265**, L39 (1983).
[13] D.C. Backer, Ann. Rev. Astron. Astrophys. **24**, 537 (1986).
[14] A.H. Jaffe and D.C. Backer, Astrophys. J. **583**, 616 (2003); J.S.B. Wyithe and A. Loeb, Astrophys. J. **590**, 691 (2003); M. Enoki, K.T. Inoue, M. Nagashima and N. Sugiyama, Astrophys. J. **615**, 19 (2004).
[15] A. Vilenkin, Phys. Lett. B**107**, 47 (1981); T. Damour and

A. Vilenkin, Phys. Rev. D**71**, 063510 (2005); S. Kuroyanagi, K. Miyamoto, T. Sekiguchi, K. Takahashi and J. Silk, Phys. Rev. D**86**, 023503 (2012); S.A. Sanidas, R.A. Battye and B.W. Stappers, arXiv:1201.2419.
[16] W. Zhao, Phys. Rev. D**83**, 104021 (2011).
[17] S. Weinberg, Phys. Rev. D**69**, 023503 (2004).
[18] W. Zhao, Y. Zhang and T.Y. Xia, Phys. Lett. B**677**, 235 (2009).
[19] L. Pages et al., Astrophys. J. Suppl. Ser. **170**, 335 (2007).
[20] H. V. Peiris et al., Astrophys. J. Suppl. Ser. **148**, 213 (2003).
[21] Y.S. Piao and Y.Z. Zhang, Phys. Rev. D**70**, 063513 (2004).
[22] L.P. Grishchuk, Lect. Notes Phys. **562**, 167 (2001).
[23] Y. Zhang, Y.F. Yuan, W. Zhao and Y.T. Chen, Class. Quant. Grav. **22**, 1383 (2005).
[24] S. Kuroyanagi, C. gordon, J. Silk and N. Sugiyama, Phys. Rev. D**81**, 083524 (2010).
[25] M.L. Tong and Y. Zhang, Phys. Rev. D**80**, 084022 (2009).
[26] Y. Watanabe and E. Komatsu, Phys. Rev. D**73**, 123515 (2006).
[27] W. Zhao and Y. Zhang, Phys. Rev. D**74**, 043503 (2006).
[28] M.S. Turner, M. White and J.E. Lidsey, Phys. Rev. D**48**, 4613 (1993).
[29] S. Chongchitnan and G. Efstathiou, Phys. Rev. D**73**, 083511 (2006).
[30] M. Giovannini, PMC Phys. A**4**, 1 (2010).
[31] M. Maggiore, Phys. Rep. **331**, 283 (2000).
[32] Here, we have transfered the value of A_s at $k_* = 0.05$Mpc^{-1} given in [6] to that at $k_* = 0.002$Mpc^{-1}.
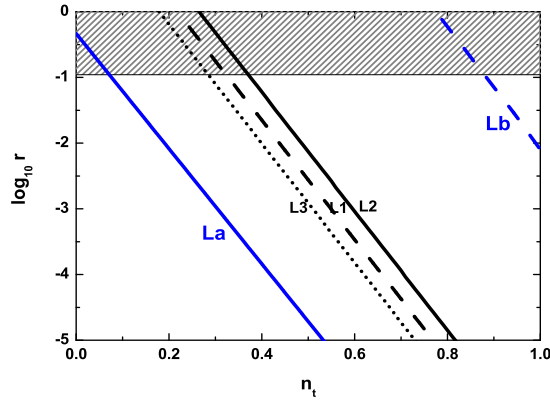
FIG. 6: The upper limits of r and n_t depend on the monitored pulsar number n. The solid black line (i.e. L2) is for the case with $n = 50$, dashed black line is for $n = 100$ (i.e. L1), and dotted black line is for $n = 200$ (i.e. L3). In all cases, $\sigma_w = 50$ns and $T = 10$yr are assumed. The solid blue line (i.e. La) and dashed blue line (i.e. Lb) are identical to those in Fig.3. The dashed black line (i.e. L1) is identical to that for SKA.

[33] L.P. Grishchuk, Physics-Uspekhi **48**, 1235 (2005).
[34] F. Jenet et al., Astrophys. J. **653**, 1571 (2006).

[35] R. van Haasteren et al., Mon. Not. Roy. Astron. Soc. **414**, 3117 (2011).
[36] P.B. Demorest et al., arXiv:1201.6641.
[37] M. Cortes, A.R. Liddle and D. Parkinson, JCAP **1109**, 027 (2011).
[38] W. Zhao and D. Baskaran, Phys. Rev. D**79**, 083003 (2009).
[39] F.A. Jenet, G.B. Hobbs, K.J. Lee and R.N. Manchester, Astrophys. J. **625**, L123 (2005).
[40] K.J. Lee, C.G. Bassa, R. Karuppusamy, M. Kramer, R. Smits and B.W. Stappers, Mon. Not. Roy. Astron. Soc. **423**, 2642 (2012).
[41] R. van Haasteren, Y. Levin, P. McDonald and T. Lu, Mon. Not. Roy. Astron. Soc. **395**, 1005 (2009).
[42] J. Ellis, X. Siemens and R. van Haasteren, arXiv:1302.1903.
[43] R. Nan, D. Li, C. Jin, Q. Wang, L. Zhu, W. Zhu, H. Zhang, Y. Yue and L. Qian, Int. J. Mod. Phys. D**20**, 989 (2011).
[44] W. Zhao, Phys. Rev. D**79**, 063003 (2009); W. Zhao and W. Zhang, Phys. Lett. B**677**, 16 (2009); Y.Z. Ma, W. Zhao and M.L. Brown, JCAP **1010**, 007 (2010); W. Zhao, JCAP **1103**, 007 (2011).
[45] P. Dewdney, Proc. IEEE **97**, 1482 (2009); A.R. Taylor, Proceedings IAU Symposium No. 291, 2012.
[46] A. Sesena and A. Vecchio, Class. Quant. Grav. **27**, 084016 (2010).
[47] The sensitivity of PTA also depends on the observing schedules, which has been detailed discussed and optimized in [40, 48].
[48] M. Anholm, S. Ballmer, J.D.E. Creighton, L.R. Price and X. Siemens, Phys. Rev. D**79**, 084030 (2009).